

DOI: 10.1002/

Article type: Full Article

### **Laser-Induced Forward Transfer: a Digital Approach for Printing Devices on Regular Paper**

*Pol Sopeña, Javier Sieiro, Juan M. Fernández-Pradas, José M. López-Villegas, Pere Serra\**

P. Sopeña, Dr. J. M. Fernández-Pradas, Prof. P. Serra  
Departament de Física Aplicada, Universitat de Barcelona, Martí i Franquès 1, 08028, Barcelona,  
Spain. E-mail: pserra@ub.edu

P. Sopeña, Dr. J. Sieiro, Dr. J. M. Fernández-Pradas, Prof. J. M. López-Villegas, Prof. P. Serra  
Institute of Nanoscience and Nanotechnology (IN<sup>2</sup>UB), Universitat de Barcelona, Av. Diagonal 645,  
08028, Barcelona, Spain.

Dr. J. Sieiro, Prof. J. M. López-Villegas  
Departament d'Enginyeries: Electrònica, Universitat de Barcelona, Martí i Franquès 1, 08028,  
Barcelona, Spain.

Keywords: Laser forward transfer, laser printing, printed electronics, paper electronics, screen printing ink.

Inkjet printing (IJP) is the most widespread direct-write technique in paper electronics. However, its use is limited, since its low-viscosity nano-inks leak through the cellulose fibers. Thus, a planarization coating is frequently used as barrier, despite that this makes substrates more expensive and less ecofriendly. Alternatively, high solid content screen printing (SP) inks could allow printing on regular paper due to their high viscosity and their large particle size; however, they cannot be printed through IJP. Another digital technique is required: laser-induced forward transfer (LIFT).

The aim of this work is to prove the feasibility of LIFT for printing devices on regular paper. The main transfer parameters are systematically varied to obtain uniform Ag-SP interconnects, which performance is improved by a multiple-printing approach, resulting in low resistances with a much better performance than those typical of IJP. After optimizing the printed lines functionality, a proof-of-concept consisting on a radio-frequency inductor is provided. The characterization of the device

shows a substantially higher performance than that of the same device printed with IJP ink in similar conditions, which proves the potential of LIFT for digitally fabricating devices on regular paper.

## 1. Introduction

Printed electronics (PE) is a cost-effective alternative to well-established silicon-based electronics that relies on the use of conventional techniques imported from the graphics industry to print components and devices.<sup>[1]</sup> Unlike silicon electronics, in PE there is a larger variety of available substrates, ranging from rigid to flexible, from inorganic to organic, and even transparent or stretchable.<sup>[2,3]</sup> Traditionally, rigid materials such as phenolic paper or woven fiber-glass impregnated with dielectric resins have been used as substrates for printed circuit boards (PCB).<sup>[4]</sup> Though being widely used, nowadays PE is aiming for flexible devices and those PCBs are being replaced by polymeric substrates such as PET, PEN or polyimide.<sup>[5-7]</sup> These plastic substrates fulfill many of the PE advantages since they are organic, low-cost and light-weight, besides being flexible. However, in the last years paper, a substrate widely used in the graphics industry, has been investigated as a potential alternative for PE. Apart from the previous properties, paper is also recyclable, renewable, ecofriendly, volatile and biocompatible,<sup>[8]</sup> which further extends its benefits as a substrate for PE. In fact, paper electronics, a branch of PE that exclusively uses paper as a substrate, is already implemented in several sectors of the industry.<sup>[9,10]</sup> For instance, paper is used as a substrate for smart labels in the packaging industry, RFID tags in contactless applications, biological and environmental sensors, solar cells, and even electrochromic white displays.<sup>[8,11-13]</sup>

In the current PE industry there are many well established techniques capable of printing fully functional circuits and components. For instance, rotogravure or rotary screen printing (SP) are ideal for long run printing at very high speeds, with wide tolerances and repeatability.<sup>[14,15]</sup> If we consider

shorter runs, flat-bed SP becomes an interesting option since it is more economical and easier to setup than roll-to-roll approaches.<sup>[16]</sup> This class of techniques allow printing inks with high solid content, which is clearly advantageous in terms of the functional properties of the resulting features.<sup>[15,17]</sup> For example, in the particular case of conductive inks –typically used for printing interconnects–, this translates into very low sheet resistances, and therefore in good electrical performance. Nonetheless, these techniques rely on the use of rolls and stencils, which fabrication is usually expensive and time consuming. Thus, when considering short-production runs, customization or defect-repair, these techniques are not probably the best option. In this regard, inkjet printing (IJP) stands out as an attractive alternative.<sup>[18]</sup> Even though a large variety of ink formulations can be printed using IJP, not all inks can be ejected through the output nozzles. Only inks having low viscosities (1-10 mPa·s) and particle sizes smaller than about 1/100<sup>th</sup> of the nozzle diameter can be routinely deposited without clogging issues.<sup>[19]</sup> The low viscosity requirement limits the loading content of the inks, which is particularly detrimental in the case of conductive inks, since such low content might easily result in too high sheet resistance.<sup>[20]</sup>

Laser-induced forward transfer (LIFT) is another direct-write printing technique which is capable of digitally printing inks using laser radiation.<sup>[21,22]</sup> In LIFT a thin layer of ink is homogeneously extended on a transparent substrate called donor, which is placed facing the receiver substrate at a convenient gap. Then, a laser pulse is focused on the donor film so that part of the ink is projected forward and transferred onto the receiver substrate.<sup>[23,24]</sup> In this way, a voxel of ink is deposited and, through the successive repetition of this process, any pattern can be reproduced on top of a wide variety of substrates, such as glass, polymers or paper.<sup>[25-32]</sup> The absence of nozzle in LIFT allows printing inks with barely no limitation in viscosity and loading particle size. Several studies have proved the feasibility of LIFT for printing liquids with low and high viscosities (from 1 to 10<sup>6</sup> mPa·s),<sup>[33-35]</sup> and suspensions containing large particles (up to 30 μm).<sup>[36-38]</sup> For instance, even though SP inks exhibit a very high viscosity (>10 Pa·s), a large particle size (a few micrometers) and a non-Newtonian rheology, which

makes them unprintable through IJP,<sup>[19,20]</sup> they could be printed using LIFT.<sup>[39-43]</sup> In addition, these type of inks are characteristic for having a very high solid content, which in the case of conductive inks translates into sheet resistances of around  $50 \text{ m}\Omega/\square$ ,<sup>[5,44-46]</sup> much lower than the common ones of IJP ( $\sim 1 \text{ }\Omega/\square$ ).<sup>[5,6,46-48]</sup> All of this makes LIFT an interesting digital alternative for printing high solid content conductive SP inks in PE applications.

In paper electronics, a common substrate of choice is coated paper. It consists on a base layer of cellulose fibers planarized with multiple layers of polymers in order to smooth and seal its surface.<sup>[8,10]</sup> This planarization step is essential when printing IJP nano-inks on paper since it avoids ink leakage through the cellulose fibers.<sup>[49,50]</sup> A more ecofriendly and cheaper alternative would be uncoated regular paper. Conductive lines cannot be printed on regular paper using IJP. However, the use of the high viscosity and large particle size inks common to SP inks would make it possible. Thus, in addition to the good functional properties stated in the previous paragraph, in the particular case of paper electronics, SP inks have the advantage that they should allow working with regular paper, which is interesting both from the economic and the environmental point of view.

In this work we prove the feasibility of LIFT for printing silver screen printing (Ag-SP) ink on paper substrates for producing conductive pads. Conductive inks are the most abundant material in printed circuitry since they serve as interconnects between the different components of any device. Therefore, printing them is fundamental for demonstrating the potential of any PE technique,<sup>[18]</sup> as we already intended in a previous work in which we printed silver nano-ink on coated paper.<sup>[51,52]</sup> Nonetheless, that was an IJP ink, which resulted in non-conductive pads when printed on regular paper. With that aim, in the current study, we print lines of high viscosity Ag-SP ink on two paper substrates: coated and regular paper. First, we systematically vary the main transfer parameters, such as the laser pulse energy, in order to find the most optimum line morphology and sheet resistance. Secondly, we consider a multiple printing approach in order to enhance the line functionality. Finally, as a proof-of-

concept, we design and print a radio frequency (RF) inductor on the two paper substrates using the Ag-SP ink, as well as a silver nanoparticle IJP ink. From a functional point of view, it is interesting to compare both inks performance on paper to ultimately explore the potential of LIFT for printing functional devices with SP inks for paper electronics.

## 2. Results and Discussion

### 2.1. Line printing

As a previous step to printing Ag-SP ink lines on paper, we printed them on glass (**Figure 1a**). Glass is a very common substrate in many electronics applications, such as displays and photovoltaic devices and, since it is very flat, smooth and rigid, printing and characterizing features on this substrate is less challenging than on paper.<sup>[11,55]</sup> In order to determine the optimum printing conditions, we varied the pulse energy from 10 to 80  $\mu\text{J}$ , maintaining a distance of 50  $\mu\text{m}$  between the centers of adjacent printed spots by setting the scan speed at the maximum (5 m/s) and the repetition rate at 100 kHz. At the lowest energy, 10  $\mu\text{J}$ , no transfer occurred, being 20  $\mu\text{J}$  the minimum pulse energy leading to transfer in our scan. At that particular energy, we obtained a thin, discontinuous and non-uniform line, clearly inappropriate for printing interconnects. At higher energies (30  $\mu\text{J}$  and above) we obtained continuous and stable lines in all cases, with a trend to become less uniform at the highest energies.

Using both confocal and optical microscopy we characterized the morphology of the printed lines and the results are plotted in Figure 1b. The line average thickness increases with pulse energy, reaching the highest value (2.3  $\mu\text{m}$ ) at 40  $\mu\text{J}$ , after which it becomes rather constant. Even though the thickness tends to saturate at a given energy, the width keeps increasing monotonously from 100 to 250  $\mu\text{m}$ , which can be attributed to a higher kinetic energy at the instant of impact of the ink on the receiver substrate. All in all, these results indicate that the amount of printed material increases with the pulse energy. This could be related to the ejection mechanism which initial propelling pressure will increase

accordingly with the pulse energy and, thus, will lead to a greater drag of material from the donor film onto the receiver.<sup>[24]</sup>

After printing, we functionalized the ink as described in Section 2. Then, we measured the sheet resistance and determined its optimal value. We found the lowest value, around  $550 \text{ m}\Omega/\square$ , for 30 and 40  $\mu\text{J}$ , which is half of the value at 50 and 60  $\mu\text{J}$ . At the lowest and highest energies (20, 70 and 80  $\mu\text{J}$ ) the measurements revealed open circuit. We performed equivalent printing experiments on both c-paper and r-paper (Figure 1a), finding similar sheet resistance values and the same optimum printing conditions at around 30 and 40  $\mu\text{J}$ . Nonetheless, the high roughness of r-paper compromised the thickness measurement of the printed features. This is the reason why the lines printed on r-paper in Figure 1a look different from the others; in order to make them visible images had to be taken in dark field configuration, otherwise they were indistinguishable from the cellulose fibers. Since c-paper presents a smoother surface we had no issues on visualizing it in bright field.

From this morphological and functional analysis, we concluded that lines printed at 30 and 40  $\mu\text{J}$  are the optimum ones for printing interconnects in electrical circuits, since they show the lowest sheet resistance. Although lines at 30  $\mu\text{J}$  are narrower than those at 40  $\mu\text{J}$ , we considered that printing at 40  $\mu\text{J}$  was more convenient; 30  $\mu\text{J}$  is an energy close to the transfer threshold, which can easily result in irregularities and defects on the lines due to the typical instabilities of lasers, as it is clear from the neck apparent in the line printed at 30  $\mu\text{J}$  on c-paper (red arrow of Figure 1a). The line width obtained at those optimum conditions, around 200  $\mu\text{m}$ , is larger than the minimum features typical of IJP,<sup>[6,48,56]</sup> but of the order of the ones corresponding to SP,<sup>[44,45]</sup> which makes it acceptable in a broad range of applications. In fact, in today PE market there are many devices, such as RFID tags, solar cell contacts, sensors or antennas, that do not require very high resolutions and easily feature interconnects hundreds of microns wide.<sup>[5,18,57-59]</sup> In any case, we could expect to obtain narrower lines by using a tighter laser beam spot and thinner donor films. The thickness and sheet resistance of the lines (2.3

$\mu\text{m}$  and  $550\text{ m}\Omega/\square$ ), are substantially better than those typically obtained with IJP (around  $0.3\text{-}1.0\text{ }\mu\text{m}$  and  $1\text{ }\Omega/\square$ ).<sup>[6,48,60]</sup> Nonetheless, comparing them with the high aspect-ratio and highly conductive lines so characteristic of SP technology, lines are still thin and resistive.<sup>[5,44-46]</sup> Besides, an estimation of the line resistivity was computed, obtaining a value of  $130\text{ }\mu\Omega\text{-cm}$ . This value is substantially above the nominal one ( $\sim 37.5\text{ }\mu\Omega\text{-cm}$ ), which suggests that particles within the line are not completely agglomerated and/or that material needs to be further compacted and more uniformly distributed. These issues are apparent in the SEM images of **Figure 2**, where the lines printed at optimum conditions on the three substrates are shown. It is clear from those images that ink is not uniformly distributed and there are abundant voids (Figure 2b). These defects compromise the line conductance and result in a higher resistivity than the nominal one in the estimation. It is also remarkable that lines printed on both glass and c-paper are completely distinguishable, whereas that is not the case for r-paper. As mentioned before, the high roughness of r-paper, caused by the  $\sim 10\text{ }\mu\text{m}$  thick cellulose fibers, complicates the proper visualization of the printed features. According to all of this, and in order to enhance the line properties, we considered adopting a multi-layer printing approach.

## 2.2. Multiple printing

Multiple-layer printing is a typical approach of digital printing techniques, especially IJP, as a strategy to enhance line uniformity and functionality –essentially, decrease sheet resistance in conductive lines–, and correct possible defects.<sup>[48]</sup> Using the previously found optimum printing conditions we printed 2 cm long straight lines consisting of up to 8 superposed layers of Ag-SP ink on glass, c-paper and r-paper. In Figure 2b SEM images of the center of those lines are shown. As the number of superposed prints increases from 1 to 4 the voids of the lines are rapidly filled until reaching a uniform coverage at 4 prints and above. Even though the substrate roughness is remarkable in the case of r-paper, once several layers are printed, no evidence of the underlying surface is detectable. Moreover, ink apparently stays on top of r-paper without massive leakage of the ink between the cellulose fibers,

which already fulfills one of the proposed objectives of the work. In **Figure 3a** the cross-sectional profile of some lines printed on glass with a different number of prints is shown. It can be observed how lines become thicker as the number of prints increases, and how their cross section gets closer to the ideal rectangular shape,<sup>[1]</sup> which contrasts with the irregular cross sections due to the coffee-ring effect, so typical of the low viscosity inks used in IJP.<sup>[8,20,48,61]</sup> The high viscosity and large particle size of the Ag-SP ink prevent significant redistribution of the ink once it is deposited by mitigating the Marangoni flow responsible for the coffee-ring effect, so detrimental for lines conductance.

We plot in Figure 3b the average thickness of the lines printed on the three substrates versus the number of prints, which shows a clear linear increase that indicates that each print stacks on top of the previously deposited material, without significant overflow. The measured thicknesses, ranging between 2 and 14  $\mu\text{m}$ , are substantially larger than those normally obtained with IJP (0.3-1.0  $\mu\text{m}$ ), even with multiple prints,<sup>[5,46]</sup> and they are perfectly comparable to the ones usually obtained with SP technology ( $\sim 15 \mu\text{m}$ ).<sup>[46,62]</sup> If we analyze the trend for the different substrates in more detail, slight differences are observed: the thickness slope for glass is slightly higher than for c-paper and r-paper, respectively. This could be explained in terms of the different roughness and porosity for each substrate (Figure 2a). Since r-paper is not planarized it contains pores between the cellulose fibers. Thus, when ink is deposited on top, it has to conform to the paper surface topography and part of the ink is dedicated to fill in those pores. In fact, the line thickness for 1 and 2 prints could not even be measured because the line was too thin to be distinguishable on such irregular surface. The non-Newtonian behavior of the ink, shown in the Experimental Section, can also play a significant role. When ink is ejected from the donor film it quickly attains high speeds that induce a significant viscosity drop due to the shear-thinning behavior. Thus, when ink reaches the r-paper substrate it can still leak a little through the pores. However, as soon as the ink loses kinetic energy it thickens and can no longer go on leaking. Thus, the material accommodates to the paper topography and the surface of the printed line is gradually homogenized. Then, as more and more material is transferred, the original

roughness of r-paper is finally suppressed, so that, on the following prints ink simply stacks on top of a previous layer of ink creating a uniform line.<sup>[63]</sup> In consequence, thickness is slightly lower on r-paper compared to the other two substrates. On the contrary, glass is completely flat, smooth and impermeable, so that ink can only pile-up on previous layers, thus obtaining thicker lines. In the case of c-paper, thanks to the planarization layer, it is smoother than r-paper, but still rougher than glass, so that the thickness of the printed lines remains between those of the other substrates.

The average width of the lines versus the number of prints is plotted in Figure 3c. We can observe the same trend for all substrates: width tends to increase and saturate as the number of prints increases. This seems reasonable since for a certain ejection velocity when the ink impacts the substrate there is a maximum spread distance. In the case of glass, saturation is attained after 3 layers are deposited, resulting in a width of around 225  $\mu\text{m}$ . C-paper has a similar behavior, with a slightly lower saturation width of 200  $\mu\text{m}$ . Finally, the width of the lines printed on r-paper saturates later, at around 5 prints, and at an even smaller value of 175  $\mu\text{m}$ . These widths are similar to the ones obtained with SP meshes.<sup>[1,8]</sup> The observed behavior can again be attributed to paper roughness, since it might easily help pinning the contact line of deposited ink and thus prevent further spreading.<sup>[64]</sup> R-paper has a rougher surface, thus, given the same initial kinetic energy, there is not as much lateral flow as in glass or c-paper since their surfaces are smoother.<sup>[65,66]</sup>

We tested the printed lines functionality by measuring their resistance. Sheet resistance versus line thickness is represented in **Figure 4a** for the three substrates. On the one hand, we can notice how the multiple-printing approach leads to a dramatic decrease in sheet resistance from around 500-700  $\text{m}\Omega/\square$  at 2  $\mu\text{m}$  thickness down to 25  $\text{m}\Omega/\square$  at 8  $\mu\text{m}$  thickness. These values are much smaller than the typical ones obtained via IJP (0.2-4.5  $\Omega/\square$ ),<sup>[5,6,46-48]</sup> and of the same order as those typical of SP, where sheet resistances of 15-70  $\text{m}\Omega/\square$  are usually achieved.<sup>[5,44-46]</sup> On the other hand, as the number of prints increases, the points gather along the same trend with no apparent difference between

substrates. This is remarkable since it proves the feasibility of LIFT for printing conductive lines even on r-paper, which actually constitutes one of the main objectives of this work. As stated before, by avoiding the need of a planarization layer, this allows reducing the costs associated with the substrate substantially, and makes the printing process more sustainable from an environmental point of view. So, in view of these results, LIFT seems a promising alternative for digitally printing SP conductive inks, with the advantage of making it possible even on r-paper, without the need for previous planarization.

In Figure 4b we represent the sheet resistance of the lines versus the inverse of thickness ( $1/t$ ). According to what we previously observed in Figure 4a, points tend to cluster at thicknesses greater than around  $5 \mu\text{m}$  ( $1/t < 0.2 \mu\text{m}^{-1}$ ) describing a linear trend. Through a linear fit we obtained a resistivity ( $\rho$ ) of  $43 \pm 6 \mu\Omega \cdot \text{cm}$ , which is in good agreement with the nominal value ( $37.5 \mu\Omega \cdot \text{cm}$ ), and therefore indicates both good line uniformity and good electrical properties. However, the plot displays significant dispersion in the experimental points corresponding to thin lines (high  $1/t$ ). These points correspond to lines with a single or just a few prints, conditions in which lines were irregular and had voids, as observed in the SEM images of Figure 2. Therefore, the diversion from the linear trend is consistent with the observed non-uniform thickness. In order to test this interpretation, we propose a simple model consisting on a Ag-SP ink line with a constant width and variable periodic thickness as represented in Figure 4c. This variable thickness, which is an oversimplification of the real case, would account for the random defects and non-uniformities observed in the lines with a few prints and should help explain the diversion from linearity. In the model, the line is composed of  $N$  segments with the same length evenly distributed along it. Half of them have a thickness  $t + \delta/2$  and the other half  $t - \delta/2$ , where  $\delta$  corresponds to the thickness of the irregularities. If we assume that this distribution is equivalent to a series resistance association, the sheet resistance can be found to be:

$$R_s = \rho \frac{t}{t^2 - \delta^2/4}. \quad (1)$$

The fit of Equation (1) to the entire set of measurements in Figure 4b, provides the behavior described by the green dashed curve. The new resistivity obtained from this fit is of  $53 \pm 5 \mu\Omega\cdot\text{cm}$ , a higher value than the one previously obtained, but still similar. From the fit, we also obtain a value of  $2.7 \pm 0.2 \mu\text{m}$  for  $\delta$ , which is similar to the average particle size of the largest silver flakes ( $0.3\text{-}10 \mu\text{m}$ ) in the ink, which in the end are responsible for the irregularities in the line profile observed at very low number of prints (Figures 2 and 3a). Therefore, and in spite of its extreme simplicity, the model helps explaining the deviation from linearity of the sheet resistance behavior at low thicknesses (low number of prints), which is caused by the variable cross section induced by the non-uniformities arising from the incomplete coverage of the lines.

### 2.3. Proof-of-concept

As a proof-of-concept for ultimately demonstrating the feasibility of LIFT for paper electronics we printed an RF inductor on the paper substrates. The inductor, which layout is shown in **Figure 5a**, consists of a square spiral inductor of six turns with a line pitch of 0.7 mm and an external guard ring on the front side of the paper substrate. The guard ring helps isolate the inductor from external electric fields that might affect the measurement. Then, a conductive bridge was printed at the back of the paper to connect the center of the coil with the outer part. In order to prove the potential of LIFT for paper electronics we printed a total of three inductors on the two paper substrates using different inks (Figure 5b). The first and second inductor consisted on Ag-SP ink printed on c-paper and r-paper at the optimum printing conditions ( $40 \mu\text{J}$ , 5 m/s and 100 kHz), labelled as  $L_{SC}$  and  $L_{SR}$ , respectively. The third inductor, named as  $L_{IC}$ , which served as a control, was printed on c-paper using Ag-NP IJP ink. Since the IJP ink has a different rheology from the Ag-SP ink, the optimum laser parameters were also different: scan speed of 5 m/s, repetition rate of 60 kHz and pulse energy of  $2 \mu\text{J}$ . In all three cases, 5 superposed prints were used, since these are the number of prints above which the lines were found to be acceptably uniform and conductive.

From an RF designer point of view, the metric of an inductor is defined by its equivalent inductance value,  $L_{eq}$ , and the quality factor,  $Q$ , i.e.,

$$L_{eq} = \frac{\Im(Z_{eq})}{j\omega} \quad (2)$$

$$Q = \frac{\Im(Z_{eq})}{\Re(Z_{eq})} \quad (3)$$

where  $Z_{eq}$  is the equivalent impedance of the inductor as a one-port device. To convert the 2-port scattering parameters of the inductor to  $Z_{eq}$ , there exist different alternatives that correspond to the way the device is excited from a source.<sup>[67]</sup> In this work, the differential impedance,  $Z_{diff}$ , was chosen, which is associated to the impedance seen by a current source differential excitation. From the scattering parameters, the actual value of  $Z_{diff}$  is given by:

$$Z_{diff} = 2Z_0 \frac{1+\Gamma_{diff}}{1-\Gamma_{diff}} \quad (4)$$

where  $Z_0$  is the characteristic impedance of the measurement system, i.e. 50  $\Omega$ , and  $\Gamma_{diff}$  is given by the next combination of the scattering parameters:

$$\Gamma_{diff} = \frac{1}{2}(S_{11} + S_{22} - S_{21} - S_{12}). \quad (5)$$

Figure 5c-e shows the comparison between the experimental and simulated plots of  $L_{eq}$  and  $Q$  vs. frequency for the three inductors and the relevant figures of merit for designers are collected in **Table 1**. In the low frequency range, the inductance is mainly a function of the component geometry; thus,

all three inductors should have a similar value. Whereas  $L_{SC}$  and  $L_{SR}$  have a similar value of 184 nH,  $L_{IC}$  has a higher value of 195 nH. This difference is related to the smaller thickness of the metal traces obtained with IJP ink, a fact that is also observed via simulation data. From a designer perspective, this frequency range where the  $L_{eq}$  trace stays flat is considered as the useful bandwidth of the component as an ideal inductor. Commonly, this value is named as  $L_{DC}$  or  $L_{flat-band}$ .

At higher frequencies, the peaking behaviour of  $L_{eq}$  is a consequence of the unwanted electrical energy stored in the component, which can be interpreted as a capacitor connected in parallel with the inductor. At the frequency where both magnetic and electric stored energies are equal, the self-resonant frequency (SRF), the component does not exhibit any reactance. Beyond the SRF, the inductor behaves as a capacitor. Therefore, this value should be as large as possible for circuit design. The SRF is recognised by the zero-crossing of either  $L_{eq}$  or  $Q$ . Due to the similar values of the dielectric properties of both substrate papers, the values of the SRF do not differ too much between the three inductors being 610, 590 and 615 MHz for  $L_{IC}$ ,  $L_{SC}$  and  $L_{SR}$ , respectively. The small discrepancies between measured and simulated data are within the tolerance of substrate and fabrication process.

The  $Q$  factor is clearly affected by the resistance of the inks. On one hand, the performance of  $L_{IC}$  is poor with a maximum  $Q$  of 2, which means that the sheet resistance of the IJP lines is higher due to the smaller achieved thickness. Notice that, whereas the tolerance of the thickness has a small impact on  $L_{eq}$ , it is of utmost importance to achieve high quality components. On the other hand, Ag-SP ink based inductors show a good performance, displaying  $Q$  peak values of 7.1 for  $L_{SC}$  and 9.4 for  $L_{SR}$ , which are high enough for RF circuit design. The difference between these two inductors is possibly due to variations on the multiple-printing process that result in different thicknesses. These results show the feasibility of LIFT for printing the Ag-SP ink, either on c-paper or r-paper, as cheap RF enabling technology, obtaining a much better performance than the IJP ink at the same printing conditions.

### 3. Conclusions

The feasibility of the LIFT of a silver high solid content screen printing (Ag-SP) ink on paper substrates has been proved by printing conductive lines to be used as interconnects for printed electronics applications. By varying the main transfer parameters, conductive lines were successfully printed in a digital fashion on glass and both coated and uncoated regular paper. Not only are these inks hardly printable through other direct-write methods, such as inkjet printing (IJP), because of their high viscosity, but also due to the large size of the particles in suspension (up to 10  $\mu\text{m}$ ), which easily results in nozzle clogging in IJP. Compared to the typical low viscosity nano-inks of IJP, Ag-SP inks do not leak through the cellulose fibers when printed on regular paper and allow obtaining conductive functional pads on this substrate. This represents a clear advantage since, aside from being an organic, flexible and recyclable substrate, regular paper is cheaper and more ecofriendly than coated paper.

The study has also proved that through a multiple-printing approach the lines functionality and uniformity is dramatically improved, obtaining high aspect-ratio lines of tens of micrometers in thickness and widths of around 200  $\mu\text{m}$  on all substrates. With this, very low sheet resistances, down to 25  $\text{m}\Omega/\square$ , were achieved, even on regular paper, a much better performance than that typically obtained through IJP. These results are comparable to those commonly obtained with screen printing, with the advantage over this technique that LIFT is a direct-write printing technology.

The feasibility of LIFT for printing electronic devices has been proved through a proof-of-concept consisting on the fabrication of a radio-frequency inductor printed on both coated and regular paper substrates. The inductors as fabricated performed accordingly to the designed pattern, with an optimal sheet resistance and operation cycle, so that they could be integrated in working circuits. The circuit printed on regular paper with Ag-SP ink exhibited a substantially better performance than a similar one

printed on coated paper with an IJP ink, which shows the potential of LIFT for the digital fabrication of printed electronic devices on non-conventional flexible substrates such as regular paper.

#### 4. Experimental Section

##### *Laser direct-write system:*

All the experiments were carried out using a diode-pumped ytterbium fiber laser (Rofin Powerline F20 Varia) working at the fundamental wavelength (1064 nm) and with a pulse duration of 100 ns. The beam had a Gaussian intensity profile with output energies as high as 90  $\mu\text{J}$ . The laser system was equipped with a set of two galvanometric mirrors allowing the laser beam to be scanned along the sample at speeds ranging from 10 to  $5 \times 10^3$  mm/s. After the galvo head, an f-theta lens of 100 mm focused the laser beam on the sample plane; the resulting beam diameter was 40  $\mu\text{m}$ . In order to print the ink, the scan speed was set at its highest value during all the experiments and the repetition rate and pulse energy were varied depending on the experiment.

##### *Inks, sample preparation and printing:*

The SP ink used in the experiments was a commercial conductive silver ink (Loctite EDAG PF 410 E&C). Its density was 2.5  $\text{g}/\text{cm}^3$ , its particle size ranged between 0.3 and 10  $\mu\text{m}$  (**Figure 6a**), its nominal viscosity was 12.7 Pa·s and its solid content 74.1%. However, since this type of ink is a non-Newtonian fluid, in order to characterize it a dynamic shear rheometer (TA Instruments Discovery HR) was used. Its viscosity was measured versus the shear rate, finding a shear-thinning behavior where viscosity varied several orders of magnitude along the explored shear rate range, from 2 to  $10^3$  Pa·s (Figure 6b).

The donor substrate was prepared by doctor-blading a 30  $\mu\text{m}$  thick film of ink on a  $26 \times 75$  mm<sup>2</sup> glass slide and it was placed above the receiver substrate at a gap of 60  $\mu\text{m}$ . The ink was later transferred on three different substrates: conventional glass (Deltalab microscope slides), coated paper (c-paper,

Argowiggins PowerCoat HD, 219 g/m<sup>2</sup>) and regular paper (r-paper, Xerox Colortech+, 160 g/m<sup>2</sup>). A detail of the two paper surfaces is presented in Figure 6c. The c-paper has a root mean squared roughness of around 0.8 μm whereas that of r-paper is around 2.5 μm, the peak-to-peak height was 4 and 25 μm, respectively. Before printing, the c-paper was placed in a conventional oven for 60 min at 150 °C to evaporate any organic substance that might affect ink adhesion to the substrate.<sup>[50]</sup> Depending on the experiment, consecutive prints were made on top of each other; in this case a fresh donor film was prepared for each run. Finally, once the ink was deposited it was baked in a conventional air circulated oven at 120 °C for 30 minutes as indicated by the ink provider. According to the product datasheet, the expected resistivity of the deposits after this process is around 37.5 μΩ·cm.

The IJP ink used in the proof-of-concept was also a commercial conductive silver ink (Sigma Aldrich ref. 736465). It consisted in a suspension of silver nanoparticles (Ag-NPs) with an average diameter of 50 nm. The ink density was 1.45 g/cm<sup>3</sup>, its viscosity 10-18 mPa·s and its solid content 30-35%. The donor film was also prepared by doctor-blading the ink on a microscope glass slide, resulting in a thickness of around 15 μm. As for the Ag-SP ink, 60 μm spacers were also used and 5 consecutive deposits were made, also refreshing the donor film in each print. A final baking step for curing the NPs at 120 °C for 30 minutes was applied, which was expected to result in a resistivity of 11 μΩ·cm according to the provider datasheet.

#### *Sample characterization:*

Line characterization was carried out using optical (Carl Zeiss model AX10 Imager.A1), confocal (Sensofar PLμ 2300) and scanning electron microscopy (SEM, JEOL J-7100). Electrical resistance measurements were carried out using a four-point probe multimeter (TTi 1906).

For the printed RF coils corresponding to the inductor of the proof-of-concept, their scattering parameters two-port response was measured with a network vector analyzer (Agilent Technologies, E5071B) in the frequency range from 1 MHz to 1 GHz using an output power of 0 dBm (1 mW). To launch the RF signal through the devices, ground-signal-ground tip probes (Cascade MicroTech, ACP-40-A-GSG-500) were placed on top of the pads of the access ports. To adjust the reference planes of the device at its input ports, a Short-Open-Load-Through calibration procedure was performed using a standard impedance substrate (Picoprobe, CS-9). The permittivity and loss tangent of both paper substrates, c-paper and r-paper, were obtained using the resonant cavity method (Damaskos Inc., Model 8 Thin Sheet Tester) due to its high accuracy (less than 2% error).

### *Electromagnetic simulation:*

The printed inductors were simulated using an in-house software based on the partial element equivalent circuit (PEEC) integral numerical method.<sup>[53]</sup> The method, firstly developed by A. Ruehli,<sup>[54]</sup> starts with the partition of the mixed potential integral equation. Only the metal regions of the device are divided in current-density cells and, separately, in charge cells forming two numerical meshes. For each current-density cell, a Kirchhoff's voltage equation arises that takes into account all electromagnetic couplings with the remaining current-density and charge cells. Both meshes are connected using the continuity equation that sets a Kirchhoff's current equation for each charge cell. In this sense, the method partitions Maxwell's equations in circuit equations. This method is especially fast for small to medium size planar devices. In addition, it is easily integrated in circuit simulators. Therefore, to help RF circuit designers, the software is embedded inside a platform for the design of RF and microwave circuits (Keysight Technologies, Advanced Design System) as a library of components.

For simulation purposes, the electromagnetic properties of the substrate must be known. As pointed out previously, the resonant cavity method was used to obtain them. In spite of the precision of this

method, it is only possible to measure the electrical properties for a discrete number of frequencies, which are related to the resonant modes of the cavity. Taking into account the dimensions of the cavity ( $43.2 \times 20.3 \times 3.8 \text{ cm}^3$ ), the minimum resonant frequency was 816 MHz, which corresponds to the  $TE_{101}$  mode. The mode  $TE_{102}$  was not useful because the electric field at the plane of the sample was null. Therefore, the next characterization frequency was 1.279 GHz, corresponding to the  $TE_{103}$  mode. No other frequencies were considered for characterization because they were beyond the resonant frequency of the implemented inductors. **Table 2** summarizes the measured values for both c-paper and r-paper substrates.

In the numerical model, the cross-section of all conductors was considered rectangular. Length and width were extracted from the footprint of the fabricated samples, whereas the thickness was adjusted from the measurement of the resistance value at DC.

#### Conflict of interest

The authors declare no conflict of interest.

#### Acknowledgements

This work was funded by MINECO of the Spanish Government: Project FLASH-PRINT (TEC2015-72425-EXP) and Project LAPER (TEC2017-83301-P). The authors thank Dr. J. Ortín for his assistance in the rheological measurements.

Received: ((will be filled in by the editorial staff))

Revised: ((will be filled in by the editorial staff))

Published online: ((will be filled in by the editorial staff))

#### References

- [1] K. Suganuma, *Introduction to Printed Electronics*, Springer-Verlag, New York, USA **2014**.
- [2] A. J. Kell, C. Paquet, O. Mozenon, I. Djavani-Tabrizi, B. Deore, X. Liu, G. P. Lopinski, R. James, K. Hettak, J. Shaker, A. Momciu, J. Ferrigno, O. Ferrand, J. X. Hu, S. Lafrenière, P. R. L. Malenfant, *ACS Appl. Mater. Interfaces* **2017**, *9*, 17226.
- [3] Q. Huang, Y. Zhu, *Adv. Mater. Technol.* **2019**, *4*, 1800546.
- [4] B. Ghosh, M. K. Ghosh, P. Parhi, P. S. Mukherjee, B. K. Mishra, *J. Cleaner Prod.* **2015**, *94*, 5.

- [5] J. F. Salmerón, F. Molina-Lopez, D. Briand, J. J. Ruan, A. Rivadeneyra, M. A. Carvajal, L. F. Capitán-Vallvey, N. F. Derooij, A. J. Palma, *J. Electron. Mater.* **2014**, *43*, 604.
- [6] T. Cheng, Y. Wu, X. Shen, W. Lai, W. Huang, *J. Semicond.* **2018**, *39*, 015001.
- [7] N. C. Raut, K. Al-Shamery, *J. Mater. Chem. C* **2018**, *6*, 1618.
- [8] D. Tobjörk, R. Österbacka, *Adv. Mater.* **2011**, *23*, 1935.
- [9] H. Liu, H. Qing, Z. Li, Y. L. Han, M. Lin, H. Yang, A. Li, T. J. Lu, F. Li, F. Xu, *Mater. Sci. Eng. R Rep* **2017**, *112*, 1.
- [10] S. Agate, M. Joyce, L. Lucia, L. Pala, *Carbohydr. Polym.* **2018**, *198*, 249.
- [11] A. Eshkeiti, A. S. G. Reddy, S. Emamian, B. B. Narakathu, M. Joyce, M. Joyce, P. D. Fleming, B. J. Bazuin, M. Z. Atashbar, *IEEE Trans. Compon. Packag. Manuf. Technol.* **2015**, *5*, 415.
- [12] H. Zhu, W. Luo, P. N. Ciesielski, Z. Fang, J. Y. Zhu, G. Henriksson, M. E. Himmel, L. Hu, *Chem. Rev.* **2016**, *116*, 9305.
- [13] F. Brunetti, A. Operamolla, S. Castro-Hermosa, G. Lucarelli, V. Manca, G. M. Farinola, T. M. Brown, *Adv. Funct. Mater.* **2019**, *29*, 1806798.
- [14] G. Grau, J. Cen, H. Kang, R. Kitsomboonloha, W. J. Scheideler, V. Subramanian, *Flexible Printed Electron.* **2016**, *1*, 023002
- [15] R. Søndergaard, M. Hösel, D. Angmo, T. T. Larsen-Olsen, F. C. Krebs, *Mater. Today* **2012**, *15*, 36.
- [16] Y. Aleeva, B. Pignataro, *J. Mater. Chem. C* **2014**, *2*, 6436.
- [17] F. C. Krebs, *Sol. Energy Mater. Sol. Cells* **2009**, *93*, 394.
- [18] R. K. Venkata, A. Venkata, P. S. Karthik, S. P. Singh, *RSC Adv.* **2015**, *5*, 77760.
- [19] A. Lee, K. Sudau, K. H. Ahn, S. J. Lee, N. Willenbacher, *Ind. Eng. Chem. Res.* **2012**, *51*, 13195.
- [20] J. Stringer, T. M. Althagathi, C. C. W. Tse, V. D. Ta, J. D. Shephard, E. Esenturk, C. Connaughton, T. J. Wasley, J. Li, R. W. Kay, P. J. Smith, *Manuf. Rev.* **2016**, *3*, 12.
- [21] P. Delaporte, A. P. Alloncle, *Opt. Laser Technol.* **2016**, *78*, 33.
- [22] P. Serra, A. Piqué, *Adv. Mater. Technol.* **2019**, *4*, 1800099.
- [23] C. B. Arnold, P. Serra, A. Piqué, *MRS Bull.* **2007**, *32*, 23.

- [24] J. M. Fernández-Pradas, C. Florian, F. Caballero-Lucas, P. Sopeña, J. L. Morenza, P. Serra, *Appl. Surf. Sci.* **2017**, *418*, 559.
- [25] I. N. Katis, J. A. Holloway, J. Madsen, S. N. Faust, S. D. Garbis, P. J. S. Smith, D. Voegeli, D. L. Bader, R. W. Eason, C. L. Sones, *Biomicrofluidics* **2014**, *8*, 036502.
- [26] A. Palla-Papavlu, T. Mattle, S. Temmel, U. Lehmann, A. Hintennach, A. Grisel, A. Wokaun, T. Lippert, *Sci. Rep.* **2016**, *6*, 25144.
- [27] M. I. Sanchez-Aniorte, B. Mouhamadou, A. P. Alloncle, T. Sarnet, P. Delaporte, *Appl. Phys. A* **2016**, *122*, 595.
- [28] C. Florian, S. Piazza, A. Diaspro, P. Serra, M. Duocastella, *ACS Appl. Mater. Interfaces* **2016**, *8*, 17028.
- [29] F. Zacharatos, M. Makrygianni, R. Geremia, E. Biver, D. Karnakis, S. Leyder, D. Puerto, P. Delaporte, I. Zergioti, *Appl. Surf. Sci.* **2016**, *374*, 117.
- [30] S. Papazoglou, I. Zergioti, *Microelectron. Eng.* **2017**, *182*, 25.
- [31] S. Surdo, R. Carzino, A. Diaspro, M. Duocastella, *Adv. Optical Mater.* **2018**, *6*, 1701190.
- [32] M. Makrygianni, A. Milionis, C. Kryou, I. Trantakis, D. Poulidakos, I. Zergioti, *Adv. Mater. Interfaces* **2018**, *5*, 1800440.
- [33] R. C. Y. Auyeung, H. Kim, S. Mathews, A. Piqué, *Appl. Opt.* **2015**, *31*, F70.
- [34] D. Munoz-Martin, C. F. Brasz, Y. Chen, M. Morales, C. B. Arnold, C. Molpeceres, *Appl. Surf. Sci.* **2016**, *366*, 389.
- [35] A. Piqué, H. Kim, R. C. Y. Auyeung, I. Beniam, E. Breckenfeld, *Appl. Surf. Sci.* **2016**, *374*, 42.
- [36] A. Palla-Papavlu, M. Dinescu, A. Wokaun, T. Lippert, *Appl. Phys. A* **2014**, *117*, 371.
- [37] A. Palla-Papavlu, M. Filipescu, S. Vizireanu, L. Vogt, S. Antohe, M. Dinescu, A. Wokaun, T. Lippert, *Appl. Surf. Sci.* **2016**, *374*, 312.
- [38] P. Sopeña, P. Serra, J. M. Fernández-Pradas, *Appl. Surf. Sci.* **2019**, *476*, 828.
- [39] E. Turkoz, A. Perazzo, H. Kim, H. A. Stone, C. B. Arnold, *Phys. Rev. Lett.* **2018**, *120*, 074501.

- [40] A. Kalaitzis, M. Makrygianni, I. Theodorakos, A. Hatziapostolou, S. Melamed, A. Kabla, F. de la Vega, I. Zergioti, *Appl. Surf. Sci.* **2019**, *465*, 136.
- [41] O. Koritsoglou, I. Theodorakos, F. Zacharatos, M. Makrygianni, D. Kariyapperuma, R. Price, B. Cobb, S. Melamed, A. Kabla, F. de la Vega, I. Zergioti, *Opt. Mater. Express* **2019**, *9*, 3046.
- [42] I. Theodorakos, A. Kalaitzis, M. Makrygianni, A. Hatziapostolou, A. Kabla, S. Melamed, F. de la Vega, I. Zergioti, *Adv. Eng. Mater.* **2019**, DOI 10.1002/adem.201900605
- [43] P. Sopeña, J. M. Fernández-Pradas, P. Serra, *Appl. Surf. Sci.* **2020**, *507*, 145047.
- [44] D. Erath, A. Filipovic, M. Retzlaff, A. K. Goetz, F. Clement, D. Biro, R. Preu, *Sol. Energy Mater. Sol. Cells* **2010**, *94*, 57.
- [45] W. J. Hyun, S. Lim, B. Y. Ahn, J. A. Lewis, C. D. Frisbie, L. F. Francis, *ACS Appl. Mater. Interfaces* **2015**, *7*, 12619.
- [46] J. F. Salmerón, A. Rivadeneyra-Torres, J. Banqueri, M. A. Carvajal, M. Agudo, *4th International EURASIP Workshop on RFID Technology* **2012**.
- [47] T. H. Joubert, P. H. Bezuidenhout, H. Chen, S. Smith, K. J. Land, *Mater. Today: Proc.* **2015**, *2*, 3891.
- [48] D. Zhu, M. Wu, *J. Electron. Mater.* **2018**, *47*, 5133.
- [49] J. Lessing, A. C. Glavan, S. B. Walker, C. Keplinger, J. A. Lewis, G. M. Whitesides, *Adv. Mater.* **2014**, *26*, 4677.
- [50] J. Arrese, G. Vescio, E. Xuriguera, B. Medina-Rodriguez, A. Cornet, A. Cirera, *J. Appl. Phys.* **2017**, *121*, 104904.
- [51] P. Sopeña, J. Arrese, S. González-Torres, J. M. Fernández-Pradas, A. Cirera, P. Serra, *ACS Appl. Mater. Interfaces* **2017**, *9*, 29412.
- [52] J. M. Fernández-Pradas, P. Sopeña, S. González-Torres, J. Arrese, A. Cirera, P. Serra, *Appl. Phys. A* **2018**, *124*, 214.
- [53] S. Ahyoune, J. Sieiro, T. Carrasco, N. Vidal, J. M. López-Villegas, E. Roca, F. V. Fernández, *Integration* **2009**, *63*, 332.
- [54] A. E. Ruehli, *IEEE Trans. Microw. Theor. Tech.* **1974**, *22*, 216.

- [55] E. Hrehorova, M. Rebros, A. Pekarovicova, B. Bazuin, A. Ranganathan, S. Garner, G. Merz, J. Tosch, R. Boudreau, *J. Disp. Technol.* **2011**, *7*, 318.
- [56] P. Q. M. Nguyen, L. P. Yeo, B. K. Lok, Y. C. Lam, *ACS Appl. Mater. Interfaces* **2014**, *6*, 4011.
- [57] D. T. Gethin, E. H. Jewell, T. C. Claypole, *Circuit World* **2013**, *39*, 188.
- [58] J. Hu, S. Wang, L. Wang, F. Li, B. Pingguan-Murphy, T. J. Lu, F. Xu, *Biosens. Bioelectron.* **2014**, *54*, 585.
- [59] Y. Liu, M. Pharr, G. A. Salvatore, *ACS Nano* **2017**, *11*, 9614.
- [60] A. Chiolerio, G. Maccioni, P. Martino, M. Cotto, P. Pandolfi, P. Rivolo, S. Ferrero, L. Scaltrito, *Microelectron. Eng.* **2011**, *88*, 2481.
- [61] J. G. V. Scott, *Circuit World* **2005**, *31*, 34.
- [62] S. L. Merilampi, T. Björninen, A. Vuorimäki, L. Ukkonen, P. Ruuskanen, L. Sydänheimo, *Proc. IEEE* **2010**, *98*, 1610.
- [63] P. Ihalainen, A. Määttänen, J. Järnström, D. Tobjörk, R. Österbacka, J. Peltonen, *Ind. Eng. Chem. Res.* **2012**, *51*, 6025.
- [64] K. Dogome, T. Enomae, A. Isogai, *Chem. Eng. Process.* **2013**, *68*, 21.
- [65] T. Seifert, E. Sowade, F. Roscher, M. Wiemer, T. Gessner, R. R. Baumann, *Ind. Eng. Chem. Res.* **2015**, *54*, 769.
- [66] B. Trnovec, M. Stanel, U. Hahn, A. C. Hübler, H. Kempa, R. Sangl, M. Forster, *Prof. Papermaking* **2009**, *6*, 48.
- [67] T. Carrasco, J. Sieiro, J. M. López-Villegas, N. Vidal, R. González-Echevarría, E. Roca, *Prog. Electromagn. Res.* **2012**, *130*, 411.

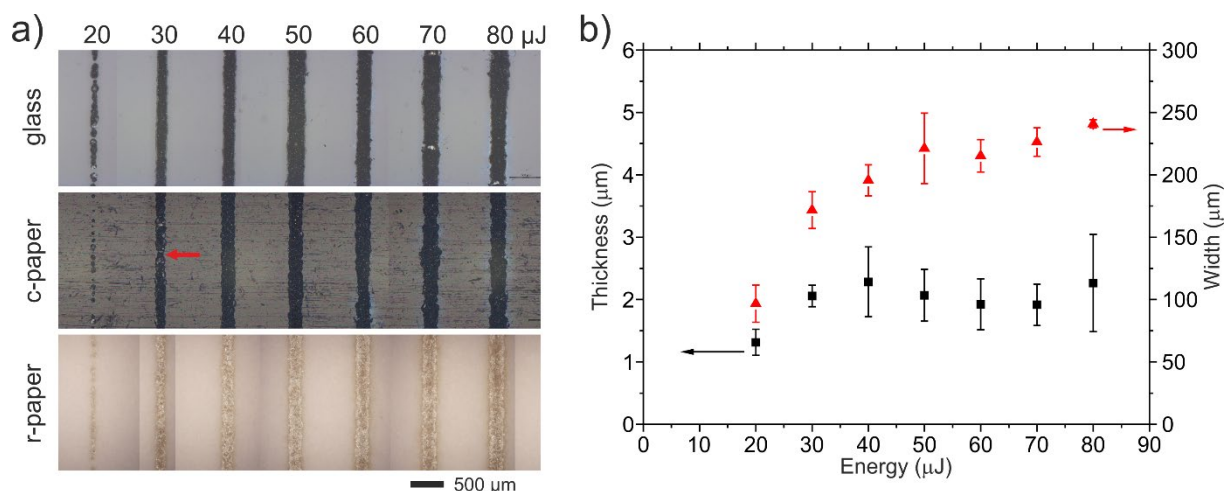


**Figure 1.** a) Optical microscope images of Ag-SP ink lines printed at several energies (indicated on top) on glass, c-paper and r-paper. The scan speed was 5 m/s and the repetition rate 100 kHz. A red arrow on the line deposited on c-paper at 30  $\mu\text{J}$  indicates a defect in the print. Images of the lines on r-paper were taken in a dark field configuration. b) Plot of the thickness and width versus the laser pulse energy for the lines printed on glass. The thickness is rather constant with a maximum of 2.3  $\mu\text{m}$  at 40  $\mu\text{J}$  whereas the width grows with the energy from 100 to 250  $\mu\text{m}$ .

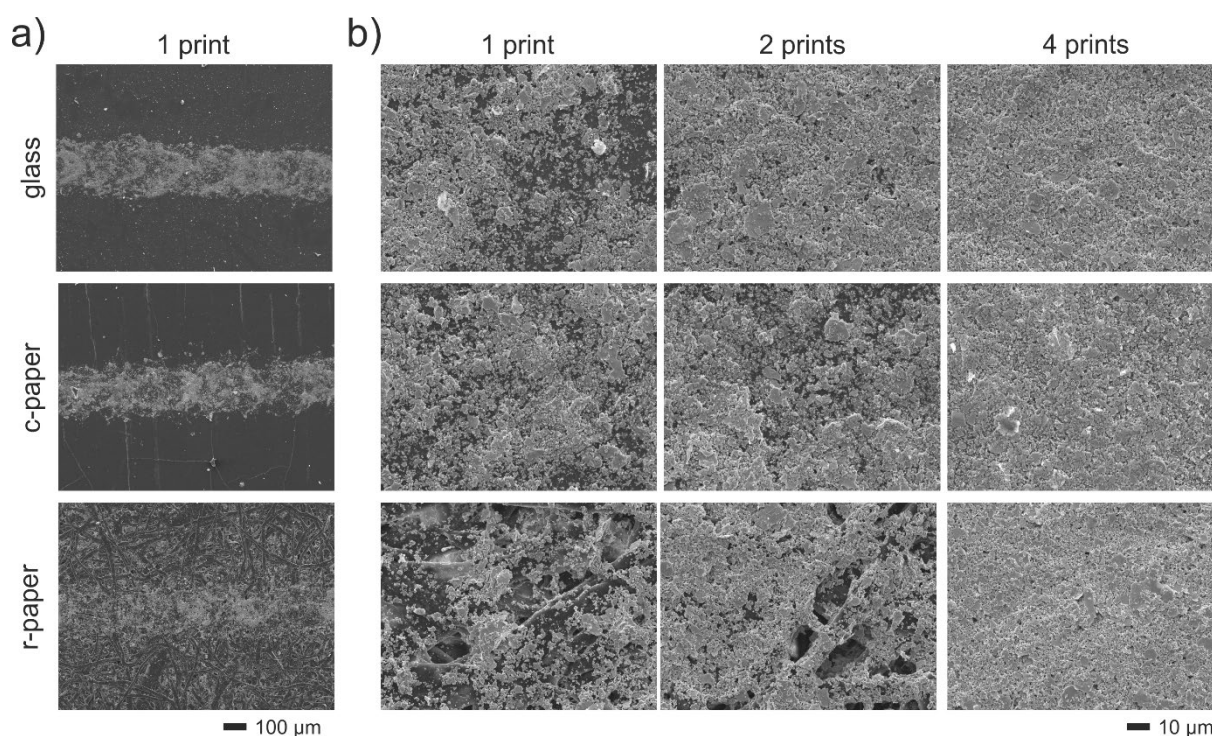


**Figure 2.** a) SEM images of single-print lines deposited on glass, c-paper and r-paper substrates. Some voids and defects can be appreciated in the lines. Glass and c-paper have a smooth surface whereas r-paper has a high roughness which complicates the visualization of the printed feature. b) Detail of the center of the lines obtained with multiple consecutive print (indicated on top) for the three substrates. As the number of prints increases the ink covers the substrate obtaining a uniform appearance at 4 prints and above. Even the high roughness of r-paper is suppressed and cellulose fibers are completely covered.

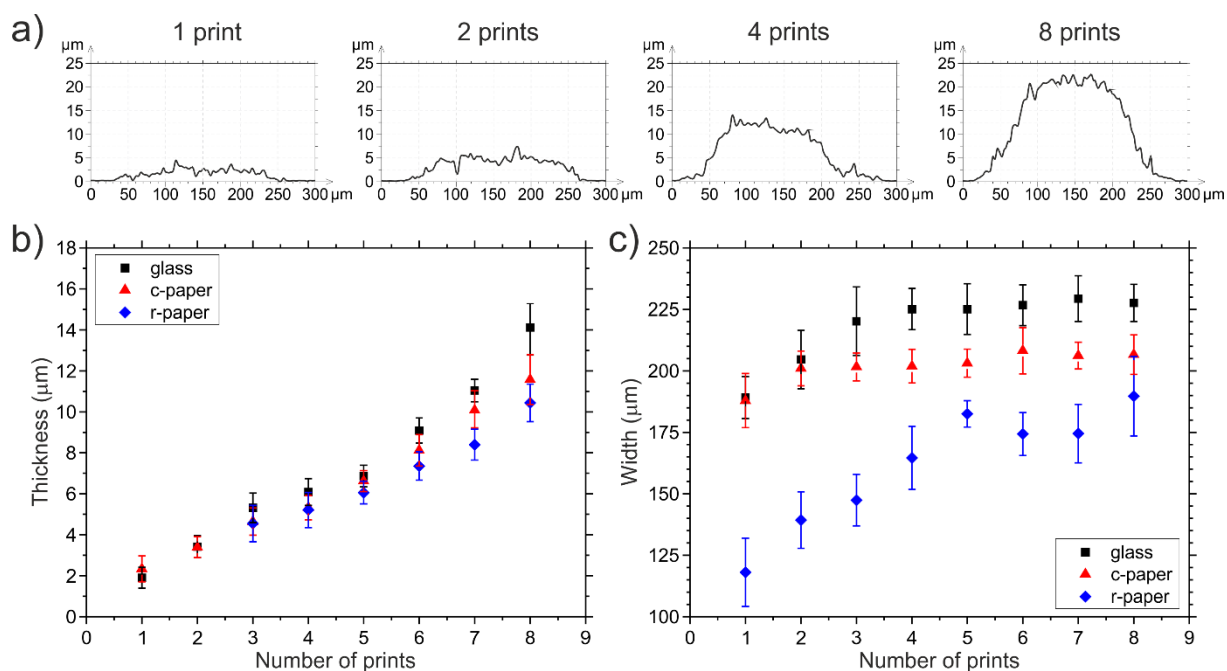


**Figure 3.** a) Line profile of Ag-SP ink lines with multiple prints (indicated on top) deposited on glass at 40  $\mu\text{J}$ , 5m/s and 100 kHz. The thickness increases with the number of prints obtaining a rather rectangular cross-section at 4 prints and above. b) Plot of the thickness versus the number of prints for the lines printed on glass (dark squares), c-paper (red triangles) and r-paper (blue diamonds). The thickness grows linearly with the number of prints, from 2 to 14  $\mu\text{m}$ . c) Plot of the line width versus the number of prints for the three substrates. The width increases with the number of prints and then stabilizes. Wider lines are obtained for glass than for r-paper, reaching a stable width of 225, 200 and 175  $\mu\text{m}$  for glass, c-paper and r-paper, respectively.

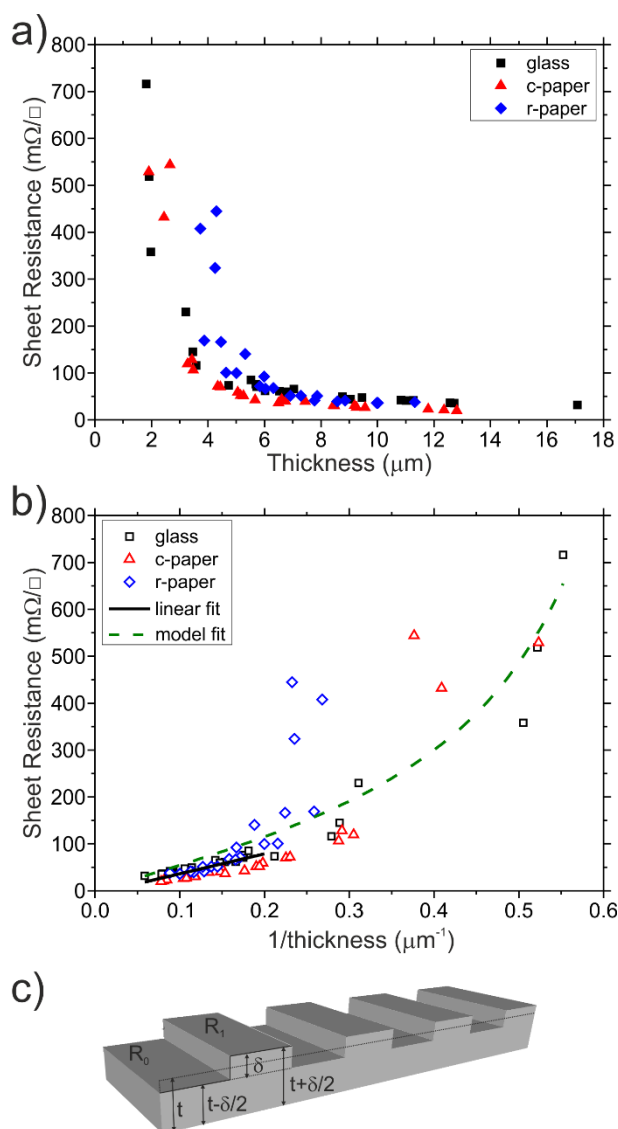


**Figure 4.** a) Plot of the sheet resistance versus the thickness for the lines printed on glass (dark squares), c-paper (red triangles) and r-paper (blue diamonds). The sheet resistance dramatically decreases with the thickness, reaching values as low as 25 mΩ/□. b) Plot of the sheet resistance in terms of the inverse of thickness for the different substrates. A linear fit (dark continuous curve) was performed at thickness values greater than 5 μm ( $1/t < 0.2 \mu\text{m}^{-1}$ ), obtaining a resistivity of  $43 \pm 6 \mu\Omega \cdot \text{cm}$ . Also, Equation (1) was fitted to all the values (green dashed curve) obtaining a resistivity of  $53 \pm 5 \mu\Omega \cdot \text{cm}$ . c) Schematic representation of an infinite solid line of thickness  $t$  composed of  $N$  equally distributed sections of constant resistivity  $\rho$  and width with a variable thickness  $\delta$ , half of which have a resistance  $R_0$  and thickness  $t - \delta/2$ , and the rest  $R_1$  and  $t + \delta/2$ .

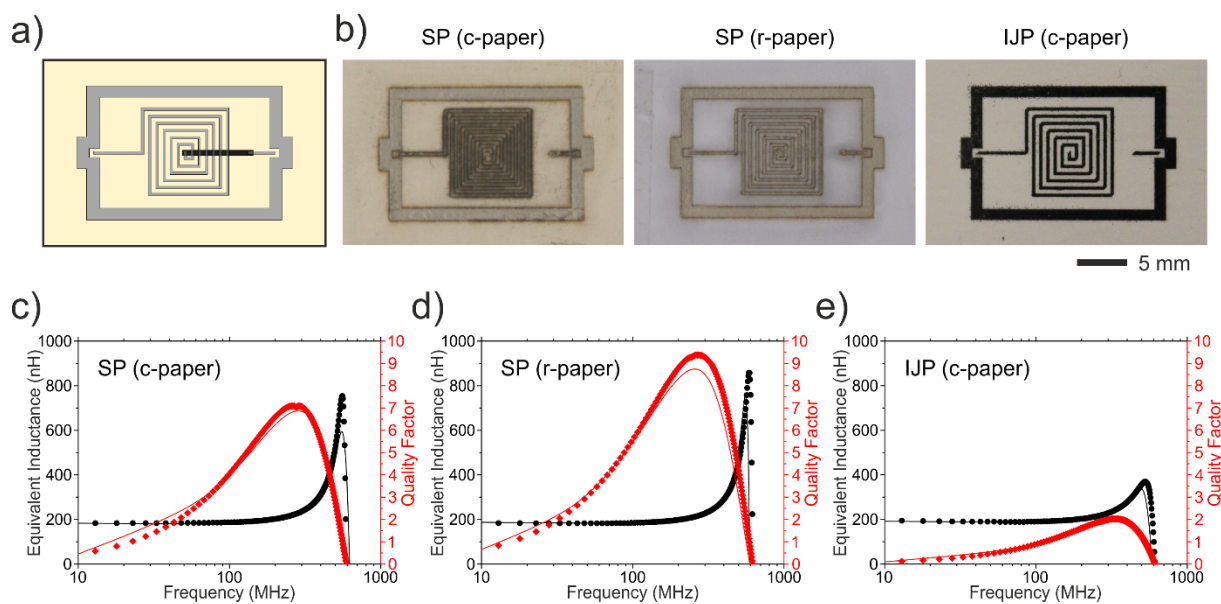


**Figure 5.** a) Schematic representation of the RF inductor layout where the grey parts correspond to the printed elements. The front side (light grey) is composed of the guard ring, the inductor and the second electrode, whereas the back side (dark grey) consists of an interconnecting bridge. b) Optical images of the three inductors: 1) Ag-SP ink printed on c-paper, 2) Ag-SP ink printed on r-paper, and 3) Ag-NP IJP ink printed on c-paper. Plots of the measured values (points) and simulated results (continuous line) of the equivalent inductance  $L_{eq}$  (black dots) and quality factor  $Q$  (red diamonds) of the c) SP ink on c-paper, d) SP ink on r-paper, and e) IJP ink printed on c-paper.

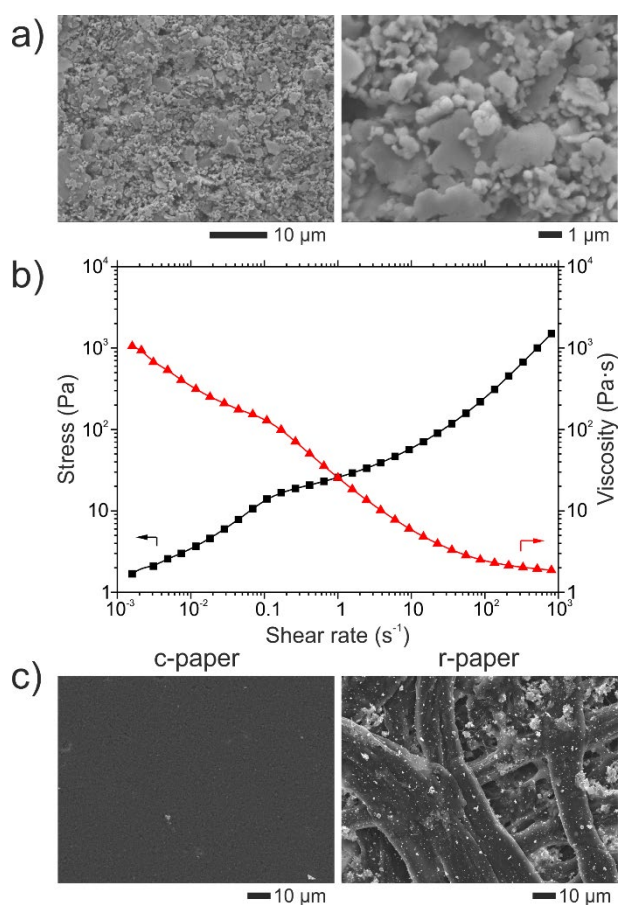


**Figure 6.** a) SEM images of the silver flakes of the SP ink once solvent has evaporated. Particle size ranges from 0.3 to 10  $\mu\text{m}$ . b) Stress (dark squares) and viscosity (red triangles) versus the shear rate of the Ag-SP ink. The viscosity describes a non-Newtonian shear-thinning behavior. c) SEM images of c-paper and r-paper substrates. The c-paper is practically smooth (roughness of 0.8  $\mu\text{m}$ ) whereas cellulose fibers with a diameter of approximately 10  $\mu\text{m}$  are completely visible for the r-paper (roughness of 2.5  $\mu\text{m}$ ).

**Table 1.** Measured relevant figures of merit for circuit designers for the three printed devices in Figure 5.

	SP c-paper	SP r-paper	IJP c-paper
$L_{\text{flat-band}}$ [nH] at 10 MHz	184	184	195
$Q_{\text{Max}}$	7.1	9.4	2.0
$f_{Q_{\text{Max}}}$ [MHz]	262	262	332
$f_0$ [MHz]	591	621	611

**Table 2.** Permittivity and loss tangent for coated and regular paper measured using the resonant cavity method.

	c-paper		r-paper	
Frequency [MHz]	816	1279	816	1279
Relative permittivity	3.61	3.54	3.87	3.68
Loss tangent	0.116	0.113	0.142	0.144